Single shot speckle and coherence analysis of the hard X-ray free electron laser LCLS

Sooheyong Lee,[1,2,3,*] W. Roseker,[2] C. Gutt,[2] B. Fischer,[2] H. Conrad,[2] F. Lehmkühler,[2] I. Steinke,[2] D. Zhu,[3] H. Lemke,[3] M. Cammarata,[3] D.M. Fritz,[3] P. Wochner,[4] M. Castro-Colin,[4] S. O. Hruszkewycz,[5] P. H. Fuoss,[5] G. B. Stephenson,[5] G. Grübel,[2] and A. Robert[3]

[1] *Korea Research Institute of Standards and Science (KRISS), Daejeon 305-600, Korea*
[2] *Hasylab at DESY, Notkestr. 85, 22607, Hamburg, Germany*
[3] *Linac Coherent Light Source, SLAC National Accelerator Laboratory, 2575 Sand Hill Road, Menlo Park, California 94025, USA*
[4] *Max-Planck-Institut fúr Intelligente Systeme, Heisenberg Straβe 3, D-70569 Stuttgart, Germany*
[5] *Materials Science Division, Argonne National Laboratory, 9700 South Cass Avenue, Argonne, Illinois 60439 USA*

**sooheyong@gmail.com*

Abstract: The single shot based coherence properties of hard x-ray pulses from the Linac Coherent Light Source (LCLS) were measured by analyzing coherent diffraction patterns from nano-particles and gold nanopowder. The intensity histogram of the small angle x-ray scattering ring from nano-particles reveals the fully transversely coherent nature of the LCLS beam with a number of transverse mode $\langle M_s \rangle$ = 1.1. On the other hand, the speckle contrasts measured at a large wavevector yields information about the longitudinal coherence of the LCLS radiation after a silicon (111) monochromator. The quantitative agreement between our data and the simulation confirms a mean coherence time of 2.2 fs and a x-ray pulse duration of 29 fs. Finally the observed reduction of the speckle contrast generated by x-rays with pulse duration longer than 30 fs indicates ultrafast dynamics taking place at an atomic length scale prior to the permanent sample damage.

OCIS codes: (030.0030) Coherence and statistical optics; (140.2600) Free-electron lasers (FELs); (300.6480) Spectroscopy, speckle.

References and links

1. M. Hogan, C. Peelegrini, J. Rosenzweig, S. Frigola, A. Tremaine, C. Fortgang, D. Nguyen, R. Sheffield, J. Kinross-Wright, A. Varfolomeev, A. Varfolomeev, S. Tolmachev, and R. Carr, "Measurement of gain larger than 10^5 at $12\mu m$ in a self-amplified spontaneous-emission free-electron laser," Phys. Rev. Lett. **81**, 4867–4870 (1998).
2. S. V. Milton, E. Gluskin, N. D. Arnold, C. Benson, W. Berg, S. G. Biedron, M. Borland, Y.-C. Chae, R. J. Dejus, P. K. D. Hartog, B. Deriy, M. Erdmann, Y. I. Eidelman, M. W. Hahne, Z. Huang, K.-J. Kim, J. W. Lewellen, Y. Li, A. H. Lumpkin, O. Makarov, E. R. Moog, A. Nassiri, V. Sajaev, R. Soliday, B. J. Tieman, E. M. Trakhtenberg, G. Travish, I. B. Vasserman, N. A. Vinokurov, X. J. Wang, G. Wiemerslage, , and B. X. Yang, "Measured exponential gain and saturation of a sase free-electron laser," Science **292**, 2037–2041 (2001).
3. S. Krinsky and Y. Li, "Statistical analysis of the chaotic optical field from a self-amplified spontaneous-emission free-electron laser," Phys. Rev. E **73**, 066501 (2006).

#193069 - $15.00 USD Received 28 Jun 2013; revised 22 Aug 2013; accepted 15 Sep 2013; published 8 Oct 2013

4. W. Ackermann, G. Asova, V. Ayvazyan, A. Azima, N. Baboi, J. Bähr, V. Balandin, B. Beutner, A. Brandt, A. Bolzmann, R. Brinkmann, O. I. Brovko, M. Castellano, P. Castro, L. Catani, E. Chiadroni, S. Choroba, A. Cianchi, J. T. Costello, D. Cubaynes, J. Dardis, W. Decking, H. Delsim-Hashemi, A. Delserieys, G. D. Pirro, M. Dohlus, S. Düsterer, A. Eckhardt, H. T. Edwards, B. Faatz, J. Feldhaus, K. Flöttmann, J. Frisch, L. Fröhlich, T. Garvey, U. Gensch, C. Gerth, M. Görler, N. Golubeva, H.-J. Grabosch, M. Grecki, O. Grimm, K. Hacker, U. Hahn, J. H. Han, K. Honkavaara, T. Hott, M. Hning, Y. Ivanisenko, E. Jaeschke, W. Jalmuzna, T. Jezynski, R. Kammering, V. Katalev, K. Kavanagh, E. T. Kennedy, S. Khodyachykh, K. Klose, V. Kocharyan, M. Körfer, M. Kollewe, W. Koprek, S. Korepanov, D. Kostin, M. Krassilnikov, G. Kube, M. Kuhlmann, C. L. S. Lewis, L. Lilje, T. Limberg, D. Lipka, F. Löhl, H. Luna, M. Luong, M. Martins, M. Meyer, P. Michelato, V. Miltchev, W. D. Möller, L. Monaco, W. F. O. Möller, O. Napieralski, O. Napoly, P. Nicolosi, D. Nölle, T. Nuñez, A. Oppelt, C. Pagani, R. Paparella, N. Pchalek, J. Pedregosa-Gutierrez, B. Petersen, B. Petrosyan, G. Petrosyan, L. Petrosyan, J. Pflüger, E. Plönjes, L. Poletto, K. Pozniak, E. Prat, D. Proch, P. Pucyk, P. Radcliffe, H. Redlin, K. Rehlich, M. Richter, M. Roehrs, J. Roensch, R. Romaniuk, M. Ross, J. Rossbach, V. Rybnikov, M. Sachwitz, E. L. Saldin, W. Sandner, H. Schlarb, B. Schmidt, M. Schmitz, P. Schmüser, J. R. Schneider, E. A. Schneidmiller, S. Schnepp, S. Schreiber, M. Seidel, D. Sertore, A. V. Shabunov, C. Simon, S. Simrock, E. Sombrowski, A. A. Sorokin, P. Spanknebel, R. Spesyvtsev, L. Staykov, B. Steffen, F. Stephan, F. Stulle, H. Thom, K. Tiedtke, M. Tischer, S. Toleikis, R. Treusch, D. Trines, I. Tsakov, E. Vogel, T. Weiland, H. Weise, M. Wellhöfer, M. Wendt, I. Will, A. Winter, K. Wittenburg, W. Wurth, P. Yeates, M. V. Yurkov, I. Zagorodnov, and K. Zapfe, "Operation of a free-electron laser from the extreme ultraviolet to the water window," Nat. Photonics **1**, 336–342 (2007).
5. T. Shintake, H. Tanaka, T. Hara, T. Tanaka, K. Togawa, M. Yabashi, Y. Otake, Y. Asano, T. Bizen, T. Fukui, S. Goto, A. Higashiya, T. Hirono, N. Hosoda, T. Inagaki, S. Inoue, M. Ishii, Y. Kim, H. Kimura, M. Kitamura, T. Kobayashi, H. Maesaka, T. Masuda, S. Matsui, T. Matsushita, X. Marchal, M. Nagasono, H. Ohashi, T. Ohata, T. Ohshima, K. Onoe, K. Shirasawa, T. Takagi, S. Takahashi, M. Takeuchi, K. Tamasaku, R. Tanaka, Y. Tanaka, T. Tanikawa, T. Togashi, S. Wu, A. Yamashita, K. Yanagida, C. Zhang, H. Kitamura, and T. Ishikawa, "A compact free-electron laser for generating coherent radiation in the extreme ultraviolet region," Nat. Photonics **2**, 555–559 (2009).
6. R. Bonifacio, L. D. Salvo, P. Pierini, N. Piovella, and C. Pellegrini, "Spectrum, temporal structure, and fluctuations in a high-gain free-electron laser starting from noise," Phys. Rev. Lett. **73**, 70–73 (1994).
7. E. Saldin, E. Schneidmiller, and M. Yurkov, "Statistical properties of radiation from vuv and x-ray free electron laser," Opt. Commun. **148**, 383–403 (1998).
8. K.-J. Kim, "Three-dimensional analysis of coherent amplification and self-amplified spontaneous emission in free-electron lasers," Phys. Rev. Lett. **57**, 1871–1874 (1986).
9. Y. Li, S. Krinsky, J. W. Lewellen, K.-J. Kim, V. Sajaev, and S. V. Milton, "Characterization of a chaotic optical field using a high-gain, self-amplified free-electron laser," Phys. Rev. Lett. **91**, 243602 (2003).
10. Z. Huang and K.-J. Kim, "Review of x-ray free-electron laser theory," Phys. Rev. ST Accel. Beams **10**, 034801 (2007).
11. P. Emma, R. Akre, J. Arthur, R. Bionta, C. Bostedt, J. Bozek, A. Brachmann, P. Bucksbaum, R. Coffee, F.-J. Decker, Y. Ding, D. Dowell, S. Edstrom, A. Fisher, J. Frisch, S. Gilevich, J. Hastings, G. Hays, P. Hering, Z. Huang, R. Iverson, H. Loos, M. Messerschmidt, A. Miahnahri, S. Moeller, H.-D. Nuhn, G. Pile, D. Ratner, J. Rzepiela, D. Schultz, T. Smith, P. Stefan, H. Tompkins, J. Turner, J. Welch, W. White, J. Wu, G. Yocky, and J. Galayda, "First lasing and operation of an ångstrom-wavelength free-electron laser," Nat. Photonics **4**, 589–591 (2010).
12. T. Ishikawa, H. Aoyagi, T. Asaka, Y. Asano, N. Azumi, T. Bizen, H. Ego, K. Fukami, T. Fukui, Y. Furukawa, S. Goto, H. Hanaki, T. Hara, T. Hasegawa, T. Hatsui, A. Higashiya, T. Hirono, N. Hosoda, M. Ishii, T. Inagaki, Y. Inubushi, T. Itoga, Y. Joti, M. Kago, T. Kameshima, H. Kimura, Y. Kirihara, A. Kiyomichi, T. Kobayashi, C. Kondo, T. Kudo, H. Maesaka, X. Maréchal, T. Masuda, S. Matsubara, T. Matsumoto, T. Matsushita, S. Matsui, M. Nagasono, N. Nariyama, H. Ohashi, T. Ohata, T. Ohshima, S. Ono, Y. Otake, C. Saji, T. Sakurai, T. Sato, K. Sawada, T. Seike, K. Shirasawa, T. Sugimoto, S. Suzuki, S. Takahashi, H. Takebe, K. Takeshita, K. Tamasaku, H. Tanaka, R. Tanaka, T. Tanaka, T. Togashi, K. Togawa, A. Tokuhisa, H. Tomizawa, K. Tono, S. Wu, M. Yabashi, M. Yamaga, A. Yamashita, K. Yanagida, C. Zhang, T. Shintake, and H. K. and N. Kumagai, "A compact x-ray free-electron laser emitting in the sub-ångström region," Nat. Photonics **6**, 540–544 (2012).
13. G. Grübel, A. Madsen, and A. Robert, "X-ray photon correlation spectroscopy," in "Soft Matter Characterization," , R. Borsali and R. Pecora, eds. (Springer-Verlag, New York, N.Y., 2008), chap. 18, pp. 954–955.
14. G. Grübel and F. Zontone, "Correlation spectroscopy with coherent x-rays," J. Alloys Compd. **362**, 3–11 (2004).
15. M. Sutton, "A review of x-ray intensity fluctuation spectroscopy," C. R. Phys. **9**, 657–667 (2008).
16. G. B. Stephenson, A. Robert, and G. Grübel, "Revealing the atomic dance," Nat. Materials **8**, 702–703 (2009).
17. J. Miao, P. Charalambous, J. Kirz, and D. Sayre, "Extending the methodology of x-ray crystallography to allow imaging of micrometre-sized non-crystalline specimens," Nature **400**, 342–344 (1999).
18. S. O. Hruszkewycz, M. Sutton, P. H. Fuoss, B. Adams, S. Rosenkranz, K. F. L. Jr., W. Roseker, D. Fritz, M. Cammarata, D. Zhu, S. Lee, H. Lemke, C. Gutt, A. Robert, G. Grübel, and G. B. Stephenson, "High contrast x-ray speckle from atomic-scale order in liquids and glasses," Phys. Rev. Lett. **109**, 185502 (2012).
19. A. Singer, I. A. Vartanyants, M. Kuhlmann, S. Düsterer, R. Treusch, and J. Feldhaus, "Transverse-coherence

#193069 - $15.00 USD Received 28 Jun 2013; revised 22 Aug 2013; accepted 15 Sep 2013; published 8 Oct 2013

properties of the free-electron-laser flash at desy," Phys. Rev. Lett. **101**, 254801 (2008).
20. A. Singer, F. Sorgenfrei, A. P. Mancuso, N. Gerasimova, O. M. Yefanov, J. Gulden, T. Gorniak, T. Senkbeil, A. Sakdinawat, Y. Liu, D. Attwood, S. Dziarzhytski, D. D. Mai, R. Treusch, E. Weckert, T. Salditt, A. Rosenhahn, W. Wurth, and I. A. Vartanyants, "Spatial and temporal coherence properties of single free-electron laser pulses," Opt. Express **20**, 17480–17495 (2012).
21. I. A. Vartanyants, A. Singer, A. P. Mancuso, O. Yefanov, A. Sakdinawat, Y. Liu, E. Bang, G. Williams, G. Cadenazzi, B. Abbey, H. Sinn, D. Attwood, K. A. Nugent, E. Weckert, T. Wang, D. Zhu, B. Wu, C. Graves, A. Scherz, J. J. Turner, W. F. Schlotter, M. Messerschmidt, J. Luning, Y. Acremann, P. Heimann, D. C. Mancini, V. Joshi, J. Krzywinski, R. Soufli, M. Fernandez-Perea, S. Hau-Riege, A. Peele, Y. Feng, O. Krupin, S. Moeller, and W. Wurth, "Coherence properties of individual femtosecond pulses of an x-ray free-electron laser," Phys. Rev. Lett. **107**, 144801 (2011).
22. W. F. Schlotter, F. Sorgenfrei, T. Beeck, M. Beye, S. Gieschen, H. Meyer, M. Nagasono, A. Fohlisch, and W. Wurth, "Longitudinal coherence measurements of an extreme-ultraviolet free-electron laser," Opt. Lett. **35**, 372–374 (2010).
23. S. Rutishauser, L. Samoylova, J. Krzywinski, O. Bunk, J. Grünert, H. Sinn, M. Cammarata, D. M. Fritz, and C. David, "Exploring the wavefront of hard x-ray free-electron laser radiation," Nat. Commun. **3**, 947 (2012).
24. A. Schropp, R. Hoppe, V. Meier, J. Patommel, F. Seiboth, H. J. Lee, B. Nagler, E. C. Galtier, B. Arnold, U. Zastrau, J. B. Hastings, D. Nilsson, F. Uhlén, U. Vogt, H. M. Hertz, and C. G. Schroer, "Full spatial characterization of a nanofocused x-ray free-electron laser beam by ptychographic imaging," Sci. Rep. **3**, 1633 (2013).
25. C. Gutt, P. Wochner, B. Fischer, H. Conrad, M. Castro-Colin, S. Lee, F. Lehmkühler, I. Steinke, M. Sprung, W. Roseker, D. Zhu, H. Lemke, S. Bogle, P. H. Fuoss, G. B. Stephenson, M. Cammarata, D. M. Fritz, A. Robert, and G. Grübel, "Single shot spatial and temporal coherence properties of the slac linac coherent light source in the hard x-ray regime," Phys. Rev. Lett. **108**, 024801 (2012).
26. D. D. Mai, J. Hallmann, T. Reusch, M. Osterhoff, S. Düsterer, R. Treusch, A. Singer, M. Beckers, T. Gorniak, T. Senkbeil, R. Dronyak, J. Gulden, O. M. Yefanov, A. Al-Shemmary, A. Rosenhahn, A. P. Mancuso, I. A. Vartanyants, and T. Salditt, "Single pulse coherence measurements in the water window at the free-electron laser flash," Opt. Express pp. 13005–13017 (2013).
27. J. Goodman, *Statistical Optics* (Wiley-Interscience, 1985).
28. M. Sutton, "Evaluation of coherence factor for high $\vec{Q}$ data," http://www.physics.mcgill.ca/ mark/coherence/yorick/highqbeta.pdf (2007).
29. P. N. Pusey, "Statistical properties of scattered radiation," in "Photon Correlation Spectroscopy and Velocimetry," , H. Z. Cummins and E. R. Pike, eds. (Plenum, New York, N.Y., 1974), pp. 45–141.
30. S. Lee, W. Roseker, C. Gutt, Z. Huang, Y. Ding, G. Grübel, and A. Robert, "High wavevector temporal speckle correlations at the linac coherent light source," Opt. Express **20**, 9790–9800 (2012).
31. J. Goodman, *Speckle Phenomena in Optics* (Roberts and Company, 2007).
32. R. B. B. McNeil and P. Pierini, "Superradiance in the high-gain free-electron laser," Phys. Rev. A **40**, 4467–4475 (1989).
33. C. Penman and B. McNeil, "Simulation of input electron noise in the free-electron laser," Opt. Commun. **90**, 82–84 (1992).
34. J. W. M. DuMond, "Theory of the use of more than two successive x-ray crystal reflections to obtain increased resolving power," Phys. Rev. **52**, 872–883 (1937).
35. L. Young, E. Kanter, B. Krassig, Y. Li, A. March, S. Pratt, R. Santra, S. Southworth, N. Rohringer, L. DiMauro, G. Doumy, C. Roedig, N. Berrah, L. Fang, M. Hoener, P. H. Bucksbaum, J. P. Cryan, S. Ghimire, J. M. Glownia, D. A. Reis, J. D. Bozek, C. Bostedt, and M. Messerschmidt, "Femtosecond electronic response of atoms to ultra-intense x-rays," Nature **466**, 56–61 (2010).
36. S. Düsterer, P. Radcliffe, C. Bostedt, J. Bozek, A. Cavalieri, R. Coffee, J. Costello, D. Cubaynes, L. DiMauro, Y. Ding, G. Doumy, F. Gruner, W. Helml, W. Schweinberger, R. Kienberger, A. Maier, M. Messerschmidt, V. Richardson, C. Roedig, T. Tschentscher, and M. Meyer, "Femtosecond x-ray pulse length characterization at the linac coherent light source free-electron laser," New J. Phys. **13**, 093024 (2011).
37. I. Tomov, P. Chen, and P. Rentzepis, "Pulse broadening in femtosecond x-ray diffraction," J. Appl. Phys. **83**, 5546–5548 (1998).
38. S. D. Shastri, P. Zambianchi, and D. M. Mills, "Dynamical diffraction of ultrashort x-ray free-electron laser pulses," J. Synchrotron Rad. **8**, 1131–1135 (2001).
39. R. Lindberg and Y. Shvyd'ko, "Time dependence of bragg forward scattering and self-seeding of hard x-ray free-electron lasers," Phys. Rev. ST Accel. Beams **15**, 050706 (2012).
40. P. K. Dixion and D. J. Durian, "Speckle visibility spectroscopy and variable granular fluidization," Phys. Rev. Lett. **90**, 184302 (2003).
41. Y. Ding, A. Brachmann, F.-J. Decker, D. Dowell, P. Emma, J. Frisch, S. Gilevich, G. Hays, P. Hering, Z. Huang, R. Iverson, H. Loos, A. Miahnahri, H.-D. Nuhn, D. Ratner, J. Turner, J. Welch, W. White, and J. Wu, "Measurements and simulations of ultralow emittance and ultrashort electron beams in the linac coherent light source," Phys. Rev. Lett. **102**, 254801 (2009).

#193069 - $15.00 USD Received 28 Jun 2013; revised 22 Aug 2013; accepted 15 Sep 2013; published 8 Oct 2013

1. Introduction

X-ray free electron lasers (XFEL) operate on the principle of self amplified spontaneous emission (SASE). They can deliver orders of magnitude more brilliant coherent radiation than previously available from synchrotron storage ring sources, tunable from VUV to the hard x-ray regime [1–5]. In a SASE FEL, the radiation produced by relativistic electrons propagates through single pass undulators where the beam modulates close to the resonance frequency of the undulator. Subsequently, the FEL collective instability induces microbunching in the electron beam and leads to the exponential growth of the radiation field before saturating [6, 7]. Due to the amplification process, which starts from the electron beam shot noise, the FEL carries different operational parameters as compared to storage ring based 3rd generation light sources. The beam is considered transversely fully coherent because the radiation is dominated by a single intense spatial mode near saturation [8]. However since a single SASE FEL pulse carries multiple temporal modes, the output spectral distribution consists of many spikes that change on a pulse-to-pulse basis [9, 10]. Therefore, a comprehensive analysis of the FEL single shot coherence properties is of fundamental interest and is a necessity to take full benefit of these new light sources.

The Linac Coherent Light Source (Menlo Park, USA) was the first FEL to demonstrate lasing in the hard x-ray regime [11] followed by SACLA (Japan) [12]. The radiation produced at these sources are suited to study structures and ultrafast dynamics in versatile condensed matter systems by means of x-ray scattering methods such as x-ray photon correlation spectroscopy [13–16] and single shot coherent diffraction imaging [17]. For example, recent results reported the feasibility of measuring high contrast single shot x-ray speckles from liquid and glasses, enabling the study of atomic length scale dynamics and structures of amorphous systems [18]. The success of these experiments relies on the accurate characterization and control of both the transverse and longitudinal coherence of the source. However, measuring the coherence of hard x-ray FEL radiation is challenging because of its sub-nanometer wavelength, femtosecond pulse duration and pulse-to-pulse intensity and spectral fluctuations.

Various attempts have been made to characterize the SASE FEL radiation. For instance, double slit and pinhole measurements are made at FLASH [19, 20] and LCLS [21] to study the coherence of these light sources. Interferometric based methods [22] were also applied to evaluate the temporal coherence. More recently, wave front properties of hard x-ray FEL pulses at LCLS have been characterized via grating interferometry [23] and ptychographic imaging [24] methods. Single shot based speckle contrast analyses have been also proposed [25, 26] to capture the coherence properties of the FEL radiation on pulse-to-pulse basis. This is highly desirable because significant longitudinal coherence fluctuation is expected due to the chaotic nature of the SASE source. In particular, our work closely follows the results reported by Gutt et al. [25], in which the speckle contrast analysis was performed on single shot diffraction images to deduce the coherence properties of the LCLS in the hard x-ray regime.

In present work, we measure the transverse coherence, in both the horizontal and vertical directions with respect to the beam path, by analyzing single shot speckle patterns in the small angle x-ray scattering (SAXS) geometry. We further probe the longitudinal coherence of the beam by monitoring the contrast fluctuations from speckle patterns at high wave vectors in the wide angle x-ray scattering (WAXS) geometry. Our analysis reveals that the LCLS beam consistently carries a high degree of spatial coherence (close to unity) while its longitudinal coherence varies on a pulse-to-pulse basis. Afterwards by applying the similar analysis on the intensity fluctuation of the LCLS output power, we evaluated the mean number of temporal modes in the beam and show that the x-ray pulse duration is indeed considerably shorter than the electron bunch duration. Later we perform 1D FEL simulation to simulate our experimental conditions and confirm the validity of our results. Ultimately, via a careful analysis of the

#193069 - $15.00 USD Received 28 Jun 2013; revised 22 Aug 2013; accepted 15 Sep 2013; published 8 Oct 2013

speckle contrasts with respect to the incoming x-ray pulse duration, we demonstrate a possibility of measuring femtosecond dynamics at an atomic length scale in the gold nanopowder sample.

2. Theory

The coherence properties of a light source can be quantified by its mutual coherence function (MCF) [27]:

$$\Gamma(\vec{r}_1,\vec{r}_2,\tau) = \left\langle \vec{E}(\vec{r}_1,t)\vec{E}(\vec{r}_2,t+\tau)\right\rangle, \tag{1}$$

where $\vec{E}(r,t)$ is the electric field at positions $\vec{r}_1$ and $\vec{r}_2$ in space and τ is the relative time delay between the two optical signals at the point of detection. The normalized MCF is known as the complex coherence function γ. It carries a value between zero (no coherence) and one (full coherence). The spatial term of the complex coherence function γ is often assumed to be a product of its horizontal and vertical components (i.e. $\gamma(t=0) = \gamma_h \cdot \gamma_v$).

When a static disordered object is illuminated by a coherent beam, the scattered radiation is not smoothly distributed in reciprocal space but instead consists of a grainy speckle pattern. The coherence properties of the radiation are encoded in the statistical properties of this pattern which can be deduced by a detailed analysis of the speckle statistics. The relation between the measured speckle contrast β and the MCF in the Fraunhofer limit can be given by [28, 29]

$$\beta(\vec{\kappa}) = \frac{1}{V^2\left\langle |\, E_i\,|^2\right\rangle^2}\int_V\int_V \exp^{i\vec{\kappa}\cdot(\vec{r}_2-\vec{r}_1)}\left|\Gamma(\vec{0},\vec{r}_2^{\perp}-\vec{r}_1^{\perp},t)\right|^2 d\vec{r}_1 d\vec{r}_2, \tag{2}$$

where $\vec{\kappa}$ specifies the displacement between two positions of detection in a scattering experiment, and V is the illuminated sample volume. In general, Eq. (2) depends on both the space and the time. Here, t is expressed as

$$t = \frac{\vec{Q}\cdot(\vec{r}_2-\vec{r}_1)}{ck_o}, \tag{3}$$

where $\vec{Q}$ is the wavevector transfer, $k_o = 2\pi/\lambda$ is the wave number, and c is the speed of light. In the Cartesian coordinate system, $\vec{Q}\cdot(\vec{r}_2-\vec{r}_1)$ is $2k_o\sin\theta\cos\theta(z_2-z_1) - 2k_o\sin^2\theta(y_2-y_1)$ in the vertical scattering plane, where θ represents the scattering angle (See Fig. 1).

The longitudinal coherence of a FEL beam is difficult to define because it is not a smooth spectrum [7, 9, 10, 30]. More specifically, a single shot SASE FEL spectrum in the frequency domain consists of multiple spikes whose width relates to the pulse duration of the radiation. Thus, we can estimate an "effective bandwidth" of the radiation based on the FWHM width of the Gaussian distribution curve. The characteristics of the polychromatic spectrum of the FEL beam in the frequency domain is modeled as a Gaussian of the form

$$S(\nu) = \frac{2\sqrt{\ln 2}}{\sqrt{\pi}\Delta\nu}\exp\left(-2\sqrt{\ln 2}\frac{\nu-\bar{\nu}}{\Delta\nu}\right)^2, \tag{4}$$

where $\Delta\nu$ is the FWHM spectral bandwidth and the Fourier transform of $S(\nu)$ yields the complex coherence function $\gamma(t)$. Since a mathematical definition of the coherence time τ_c is given by

$$\tau_c = \int_{-\infty}^{\infty}|\gamma(t)|^2\,dt, \tag{5}$$

$\gamma(t)$ can be written as

$$\gamma(t) = \exp\left(-\frac{\pi}{2}\left(\frac{t}{\tau_c}\right)^2\right), \tag{6}$$

#193069 - $15.00 USD Received 28 Jun 2013; revised 22 Aug 2013; accepted 15 Sep 2013; published 8 Oct 2013

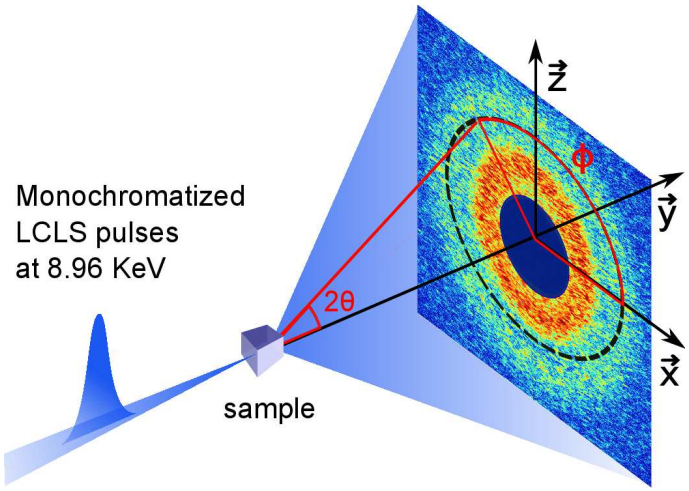

Fig. 1. Experimental schematic of our single shot coherence measurement. A single, focused monochromatized x-ray pulse is delivered to the sample in a transmission scattering geometry. For the SAXS experiment, colloidal nanoparticles are used as scattering medium while gold nanopower is used for the WAXS measurement. Here x, z and y are defined as horizontal, vertical and collinear directions to the incident beam respectively. θ and ϕ each represents the scattering angle and the azimuthal angle with respect to the incident x-rays.

where t is the time delay that corresponds to the path length difference of the scattered x-rays. For further analysis, we use a Cartesian coordinate system to describe our WAXS geometry where x, z and y are defined as horizontal, vertical and collinear directions to the incident beam respectively as shown in Fig. 1. In this case, the MCF is expressed as

$$|\Gamma(x_1,z_1,x_2,z_2,t)|^2 = V^2 \left\langle |\, E_i \,|^2 \right\rangle^2 \times e^{-\frac{(x_2-x_1)^2}{\xi_h^2}} e^{-\frac{(z_2-z_1)^2}{\xi_v^2}} e^{-t^2/2\tau_c^2}, \tag{7}$$

where ξ_h and ξ_v are the transverse coherence lengths in the horizontal and vertical directions respectively and $c\tau$ is the longitudinal coherence length assuming a Gaussian spectral profile. Finally the speckle contrast can be rewritten in terms of the coherence length and time as

$$\beta = \int_V \int_V e^{-\frac{(x_2-x_1)^2}{\xi_h^2}} e^{-\frac{(z_2-z_1)^2}{\xi_v^2}} e^{-t^2/2\tau_c^2}. \tag{8}$$

Once the transverse coherence lengths are measured, the coherence time τ_c can be numerically obtained by solving Eq. (8). The validity of the Gaussian approximation for the radiation spectrum will be discussed later by comparing the simulation result to the experimental data.

In the SAXS geometry, the typical longitudinal path length differences between the scattered radiation are about $10^{-9} \sim 10^{-10}$ m. Since the path length differences are much shorter than the expected longitudinal coherence length ($\sim$1 μm) of the 8.96 keV radiation downstream of a Si (111) monochromator, the MCF will not contain any significant time dependence. The speckle contrast β will therefore be a measure of the transverse coherence properties only (given that the speckle features can be fully resolved by a detector with sufficient spatial resolution). In the WAXS geometry, the relation between the speckle contrast and its MCF is more complex because the maximum path length difference between x-rays from the illuminating volume to the

#193069 - $15.00 USD Received 28 Jun 2013; revised 22 Aug 2013; accepted 15 Sep 2013; published 8 Oct 2013

detector is comparable to the longitudinal coherence length of the incident monochromatized beam.

3. Materials and methods

This experiment was conducted at the XPP instrument of LCLS at SLAC National Accelerator Laboratory. The electron bunches are generated at 10 Hz from a photocathode and then accelerated by a linac up to 14.2 GeV. At this point, the electron bunch duration is about 100 fs (FWHM). A single electron bunch is selected by a deflecting magnet that is triggered by an electronic signal from the end user. Subsequently the electron bunch propagates through a 70 m long undulators to generate a single x-ray pulse via the SASE process. Each x-ray bunch travels through a channel cut monochromator with Si (111) crystals operating in the vertical scattering geometry, which for this experiment delivered x-rays with an energy of E = 8.96 keV and a resolution of $\Delta E/E = 1.41 \times 10^{-4}$. After the monochromator, a typical x-ray bunch contains up to 1×10^{11} photons within its sub-100 fs pulse width. We note that the initial size of the LCLS beam (approximately 1×1 cm^2) is reduced after upstream X-ray slits during the experiment. Finally, the slitted 300×300 μm^2 size beam is focused using a beryllium refractive lens to a spot size of 3 (horizontal) $\times$ 9 (vertical) μm^2 at the sample position.

The schematic of the single shot scattering measurement is shown in Fig. 1. The diffraction signals from the sample are recorded with a direct illumination CCD (Princeton Instrument LCX) consisting of 1300×1340 pixels of 20×20 μm^2 size. The detector was placed at 4.5 m and 1.55 m away from the sample to measure speckle patterns in the SAXS and WAXS geometries respectively. Successive single shot images were taken by translating the samples after each shot to avoid damaged area on the sample from previous shots. In the SAXS geometry, the sample consists of hard sphere colloidal particles (volume fraction $\Phi = 52\%$ and size polydispersity of 16%) of 100 nm diameter. For the WAXS geometry, gold nanopowder samples were prepared by mixing a solution of Au and polyvinylpyrrolidone (PVP) on a thin kapton support. The sample thicknesses are kept at 2.24 ± 0.36 μm to ensure the reproducibility of the coherence measurement.

4. Result and discussion

4.1. Speckle statistics in SAXS geometry: Transverse coherence measurement

Series of single shot speckle patterns from the colloidal suspension are measured in the SAXS configuration. Figure 2 (left half) shows a typical single shot scattering pattern. The grainy structures on the concentric ring is a characteristic of a well developed speckle pattern and is also indicative of the highly coherent nature of the source. The individual speckles from each single shot patterns present an anisotropic aspect ratio. This feature is due to the size of the focused beam at the sample, which is inversely proportional to the speckle size. On the other hand, Fig. 2 (right half) is a multi-shot average scattering pattern that provides similar results as would be obtained with illumination by an incoherent source. It shows smooth concentric rings that are the signature of the diffraction pattern from spherical particles with a well defined diameter. For the speckle contrast evaluation at a given wave vector, we selected a region of interest consisting of an annulus of radius Q = 0.05 nm^{-1} and width $dQ \cong 0.001$ nm^{-1} (corresponding to 3$\sim$5 pixel width). The intensity fluctuation in the selected region is then evaluated by fitting the histogram of the normalized intensity by the gamma probability density distribution function [31]

$$P(I) = \frac{\Gamma(I + M_{speckle})}{\Gamma(I+1)\Gamma(M_{speckle})} \left[1 + \frac{M_{speckle}}{\langle I \rangle}\right]^{-I} \left[1 + \frac{\langle I \rangle}{M_{speckle}}\right]^{-M_{speckle}}, \quad (9)$$

#193069 - $15.00 USD Received 28 Jun 2013; revised 22 Aug 2013; accepted 15 Sep 2013; published 8 Oct 2013

where I is the number of photon events measured on the CCD and the parameter $M_{speckle}$ is a number of speckle modes corresponding to the ratio between the scattering volume and coherence volume and is related to the speckle contrast by $\beta = 1/\sqrt{M_{speckle}}$.

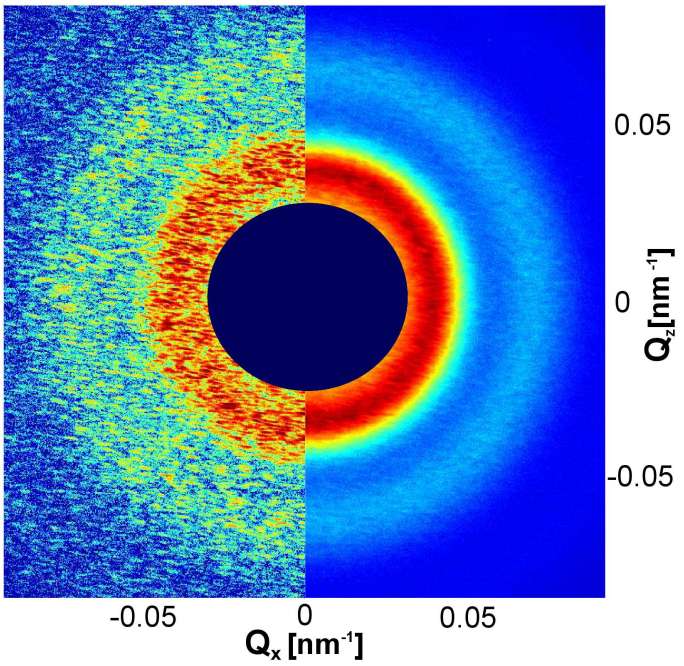

Fig. 2. X-ray diffraction pattern from the colloidal sample. A single shot coherent pattern is shown on the left. It shows strong spatial intensity fluctuation as compared to the scattering ring obtained from a sum of 50 successive shots (right half). The circular shadow in the middle is the beam stop that prevents the direct beam from reaching the detector

Figure 3(a) shows the histogram of the normalized intensity distribution at Q = 0.05 nm^{-1}. The solid line (red) is a fit to the experimental data using Eq. (9). Here since $M_{speckle}$ is only sensitive to the transverse coherence of the beam, we note the number of transverse mode as M_s. The fit yields the number of transverse mode M_s = 1.32$\pm$0.09, which corresponds to β = 0.87$\pm$0.03. The same analysis was extended to the various Q's accessible in the CCD image. In Fig. 3(b), the number of speckle modes does not display any Q dependence. In terms of the speckle contrast β the mean value is 0.87 $\pm$ 0.01 with wavevectors ranging from Q = 0.03 nm^{-1} to 0.07 nm^{-1} as shown in Fig. 3(c). Overall, an average β values measured at Q = 0.05 nm^{-1} from 90 individual shots at shows $\langle\beta\rangle$ = 0.94 $\pm$ 0.03, which demonstrates the nearly full transverse coherence of a LCLS pulse with a small fluctuation.

We further extend the study to investigate the transverse coherence along the horizontal and vertical directions. As presented in Fig. 4(a), we selected 2 regions of interest, indicated by rectangular regions H and V, for calculating the speckle contrast along z and x axes simultaneously at Q = 0.05 nm^{-1}. Here the contrast in the horizontal and vertical direction is a measure of the horizontal (γ_h) and vertical (γ_v) degree of transverse coherence. For each x-ray pulse, the speckle contrast is evaluated by fitting a normalized intensity distribution of the scattered x-rays to Eq. (9). Figure 4(b) shows a series of single shot speckle contrasts evaluated along the horizontal and vertical directions as a function of shot number. This gives average contrast values of 0.96 $\pm$ 0.04 and 0.97 $\pm$ 0.04 for the horizontal and vertical directions respectively. We do not

#193069 - $15.00 USD Received 28 Jun 2013; revised 22 Aug 2013; accepted 15 Sep 2013; published 8 Oct 2013

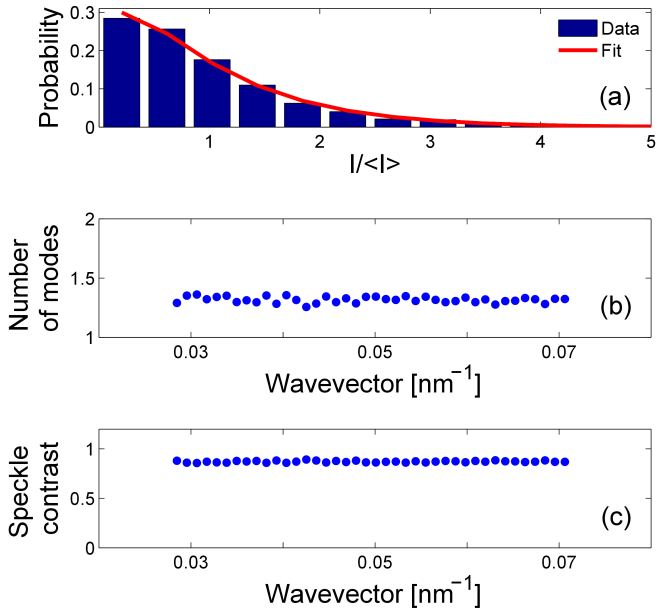

Fig. 3. (a) A probability density distribution function of intensity fluctuations of a single x-ray scattering image at an annulus of $Q = 0.05$ nm^{-1} (blue bar), which is plotted against its fitted gamma density function (solid red). Number of speckle modes (b) and speckle contrasts (c) are evaluated as a function of the wave vector Q for the same scattering pattern.

observe any significant difference between the two directions and both results show nearly full transverse coherence on average. Here, the single shot transverse coherence ($\gamma = \gamma_h \cdot \gamma_v$) is evaluated as 0.93 ± 0.06, which is consistent with the single shot coherence measurement discussed previously. We note that the fluence of 4×10^5 mJ/cm^2 from the bandpassed x-ray radiation exceeds the damage threshold of the colloidal particles. However, the SAXS diffraction pattern corresponds to relatively large length scale (hundreds of nanometers), and thus we expect no dynamics on femtosecond time scales. Therefore the FEL pulses should effectively probes a static or "frozen" system.

4.2. Speckle statistics in WAXS geometry: Longitudinal coherence measurement

The longitudinal coherence length ξ_c can be calculated from the effective bandwidth of the FEL spectrum ($\Delta\lambda/\lambda$). In a typical SAXS experiment, the path length difference P of the scattered radiation is negligible as compared to ξ_c. However at sufficiently large angles, the path length difference becomes closer to the expected longitudinal coherence length as shown in Fig. 5. Since the time delays between scattered radiation is now comparable to the coherence time given by Eq. (3), the speckle contrast in the WAXS geometry is sensitive to the longitudinal coherence properties of the incident radiation.

In our experiment, in order to quantify the temporal coherence contribution in the speckle contrast, the single shot WAXS measurements were performed on the gold nanopowder sample. The 2D area detector was positioned at a scattering angle of 34° (corresponding to Q = 26 nm^{-1}) to collect scattered x-rays from a diffraction ring from the (111) lattice plane of the amorphous sample. Figure 6(a) shows an 1D projection of the normalized scattering pattern. For the analysis, we used a region of interest indicated by two dashed red lines consisting

#193069 - $15.00 USD Received 28 Jun 2013; revised 22 Aug 2013; accepted 15 Sep 2013; published 8 Oct 2013

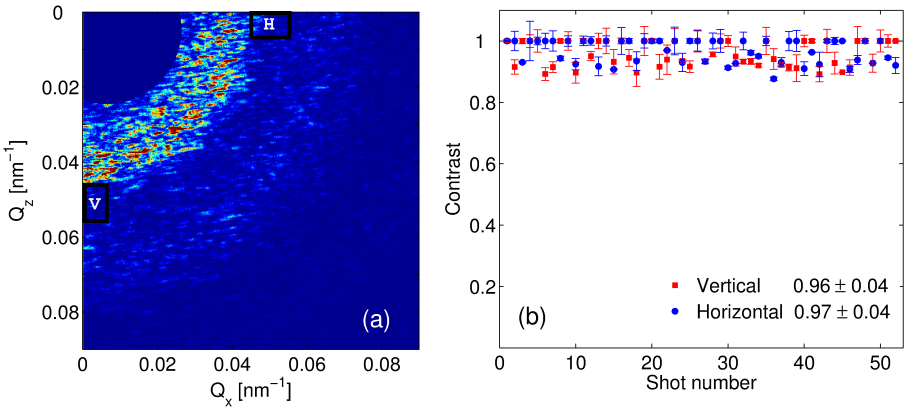

Fig. 4. (a) Regions of interest that are used for calculating speckle contrast along the vertical and horizontal directions are marked by rectangular regions H and V both at $Q = 0.05$ nm^{-1}. (b) Speckle contrast along the vertical and horizontal direction is plotted against shot number.

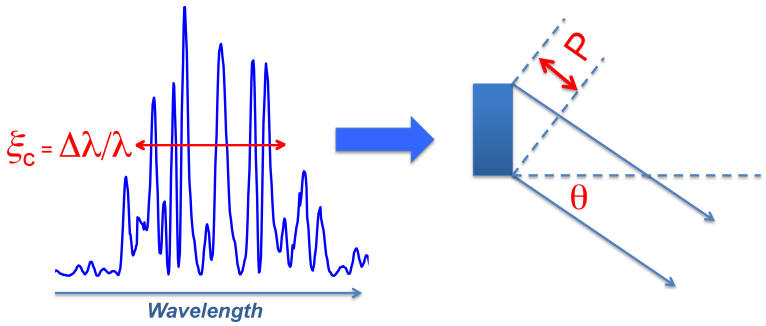

Fig. 5. An incident FEL pulse carries an effective longitudinal coherence length defined by $\xi_c = \Delta\lambda/\lambda$. In the WAXS experiment, one can match the path length difference of the scattered radiation P to ξ_c by increasing the scattering angle θ.

of 100 by 200 pixels. Figure 6(b) shows a single shot x-ray photon distribution on the CCD in the region of interest near the diffraction ring, in which 840 analog-to-digital unit (ADU) corresponds to a single photon event as shown in Fig. 6(b) inset. Scattering signals from the amorphous ring consists of mostly 1-5 discrete photon events. We note that a typical image used in our analysis has a mean count of 0.03 photons per pixel.

Figure 7(a) shows a photon event distribution in the region of interest that is measured from a single diffraction image. The solid red line is the fit to the experimental data, from which we deduce $M_{speckle} = 5$ using Eq. (9). Even at this low photon counting rate, the distribution curve is clearly different from a single mode case, which is calculated assuming $M_{speckle} = 1$ (shown in dashed green). We applied this fitting analysis routine to successive single shot images to calculate the number of speckle modes. In Fig. 7(b), unlike the SAXS result, we immediately observe the presence of multiple modes in single shot speckle images with significant shot to shot fluctuation. Subsequently, the speckle contrasts are calculated via relation $\beta = 1/\sqrt{M_{speckle}}$. As shown in Fig. 7(c), we observe the speckle contrast fluctuation between 0.1 and 0.47 with a mean contrast of $\langle\beta\rangle = 0.26 \pm 0.02$.

#193069 - $15.00 USD Received 28 Jun 2013; revised 22 Aug 2013; accepted 15 Sep 2013; published 8 Oct 2013

The speckle contrast is not directly related to the MCF of the x-rays, as it is more closely related to the ratio between the coherence volume and the scattering volume. The coherence time, however, can still be deduced from the contrast measurements by solving Eq. (2). Since the beam is transversely coherent (β = 0.93) with marginal pulse-to-pulse fluctuation, the transverse coherence contribution in MCF can be considered as a constant factor. Subsequently, Eq. (2) simplifies to

$$\beta = \int_V \int_V \exp(-(t^2/2\tau^2)). \tag{10}$$

A numerical inversion of Eq. (10) yields an estimate of the coherence time, which fluctuates about its nominal value of 2.2 fs with a standard deviation of 1.8 fs. The severe fluctuation of the coherence times reflects the SASE nature of the source where the spectrum of a single pulse carries a very different intensity and spectral profile with respect to subsequent pulses.

4.3. Comparison between high wavevector speckle statistics and FEL simulation

In order to acquire a more in-depth understanding of how the spectral properties of the LCLS beam influence the speckle statistics at high wavevector values, we performed one dimensional FEL simulation. It is based on a time-dependent approach that has been previously reported [32] along with a shot noise algorithm [33]. In the 1D simulation, the initial E_x field produced in the first undulator is propagated freely without electron beam interaction. Subsequently the electron distribution from the first undulator is used to calculate E_y field in the second undulator and so on. Table 1 shows input parameters used in our simulation.

The theoretical estimates of the speckle contrast at Q = 26 nm^{-1} and the coherence times are compared to the experimental data. Figure 8(a) shows a single shot simulated unfiltered radiation (pink beam) spectrum based on the operational parameters used in our experiment. The pink beam spectrum has an approximate bandwidth of 0.1%. The Si (111) crystal monochro-

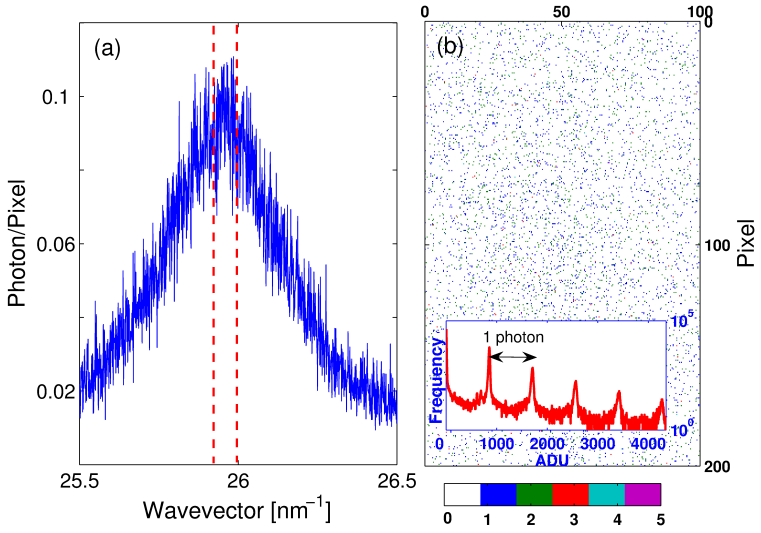

Fig. 6. (a) A single shot scattering from (111) gold nanopowder diffraction ring. The scattering angle of 2θ = 34° corresponds to $Q = 26$ nm^{-1}. Data points that lie between the dashed lines are used for the contrast evaluation. (b) A photon probability distribution in the region of interest shows that 840 ADU from the detector corresponds to a single photon event.

#193069 - $15.00 USD Received 28 Jun 2013; revised 22 Aug 2013; accepted 15 Sep 2013; published 8 Oct 2013

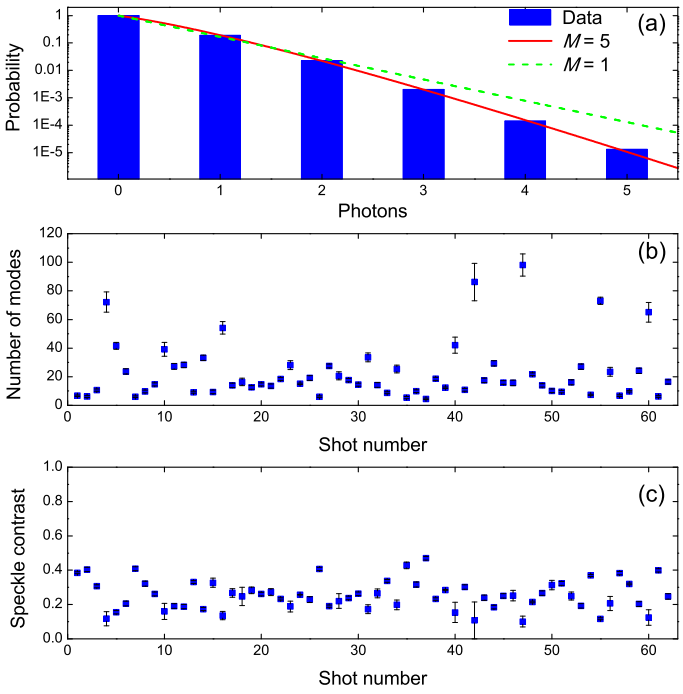

Fig. 7. (a) A histogram of the intensity distribution within the region of interest is fitted against the negative binomial distribution. The dashed green line shows the distribution curve assuming $M_{speckle}$ = 1 while the red line is the fit to the experimental data (blue square). Single shot speckle modes and contrast at Q=26 nm^{-1} for successive x-ray pulses are shown in (b) and (c), respectively.

Table 1. Input parameters for 1D FEL simulation

Electron beam energy [GeV]	14.2
Bunch peak current [kA]	2.53
Transverse normalized emittance [μm]	1.1
Undulator period [cm]	3
Undulator parameter K	3.5
FEL wavelength [Å]	1.38
FEL ρ parameter	4.13e-4
Total undulator length [m]	70

mator selects a smaller band ($\Delta E/E = 1.41\times10^{-4}$) of the spectrum. The effect of monochromatization is calculated using the DuMond approach [34], in which the Bragg reflected intensity is determined from the overlap between the source divergence and the intrinsic bandwidth of the monochromator single crystal. The transmitted spectrum through the monochromator is indicated in red in Fig. 8(a). Afterwards, the temporal part of the calculated MCF is obtained by taking the Fourier transform of the spectrum as shown in Fig. 8(b). The MCF profiles change dramatically depending on the particular features of the spectrum. For example, in the pink beam case, the FWHM of the complex coherence function is found at the x-ray path length difference that corresponds to a time delay of about 0.5 fs while the spectrum after Si (111), in

#193069 - $15.00 USD Received 28 Jun 2013; revised 22 Aug 2013; accepted 15 Sep 2013; published 8 Oct 2013

contrast, has a considerably longer coherence time of 2 fs.

Figure 9 shows the comparison between the coherence time measured in the experiment and the numerical simulation. Generally, the FEL spectrum overfills the bandwidth of the monochromator crystal. When this condition is met, the coherence time fluctuates around 2 fs for both the experiment and the simulation. However occasional x-ray pulses occur which deliver considerably higher degrees of temporal coherence (up to 10 fs in the experiment) and thus yield also higher speckle contrast.

As shown in Fig. 8(a), the output spectral structure of the pink beam consists of a large number of sharp spikes (or temporal modes). The intensity fluctuation after the Si (111) monochromator becomes considerably more pronounced as compared to the pink beam case due to fewer number of the temporal modes being transmitted (i.e. tens of spikes instead of hundreds). According to our simulations, a high degree of coherence can be achieved when a single dominant spectral mode as shown in Fig. 9 (a), or a few closely adjacent intense modes are transmitted through the monochromator. The single mode profile is ideal for performing coherent x-ray diffraction because it provides the longest coherence time and thus the most longitudinally coherent beam. In contrast, spectral profiles carrying multiple temporal modes, which overfill the monochromator bandwidth, result in relatively short coherence time as can be seen in Fig. 9(b). With SASE radiation, the intensity fluctuations after the monochromator are considerably more pronounced in the single mode transmission case. After over 1000 iterations, our simulations yield mean coherence time of $\langle \tau_c \rangle$ = 2.34 $\pm$ 1.1 fs, which is consistent with the experimental result. This value corresponds to a Gaussian energy bandwidth (FWHM) of $\Delta E/E = (1.41 \pm 0.66) \times 10^{-4}$, which is consistent with the energy bandwidth of the Si (111) monochromator. Ultimately, we find that the approximate lower limit of the coherence time is set by the monochromator bandwidth.

The fluctuation of the speckle contrast due to the FEL spectral fluctuation is calculated using Eq. (2). The MCF can be directly calculated from the Fourier Transform of the single shot

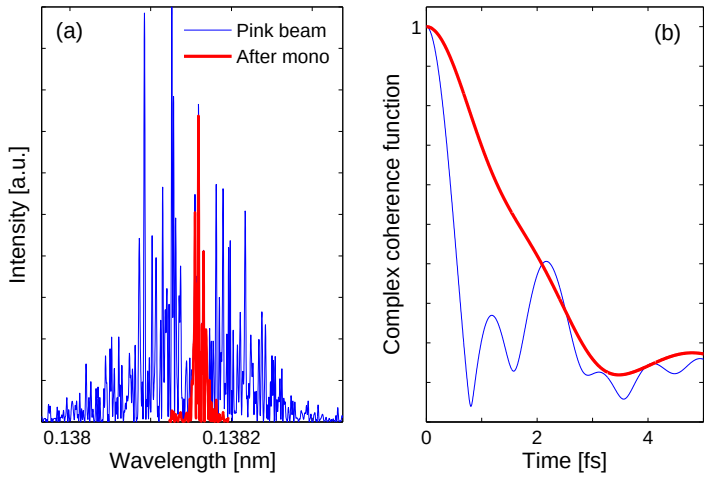

Fig. 8. (a) A single shot FEL spectrum generated from the 1D-FEL simulation under the operational parameters of LCLS (blue). The red line shows a selected portion of the spectrum after Si (111) monochromator. (b) The coherence time of the pink beam (blue) is 0.5 fs while the filtered spectrum (red) produces a considerably longer coherence time of 2 fs.

#193069 - $15.00 USD Received 28 Jun 2013; revised 22 Aug 2013; accepted 15 Sep 2013; published 8 Oct 2013

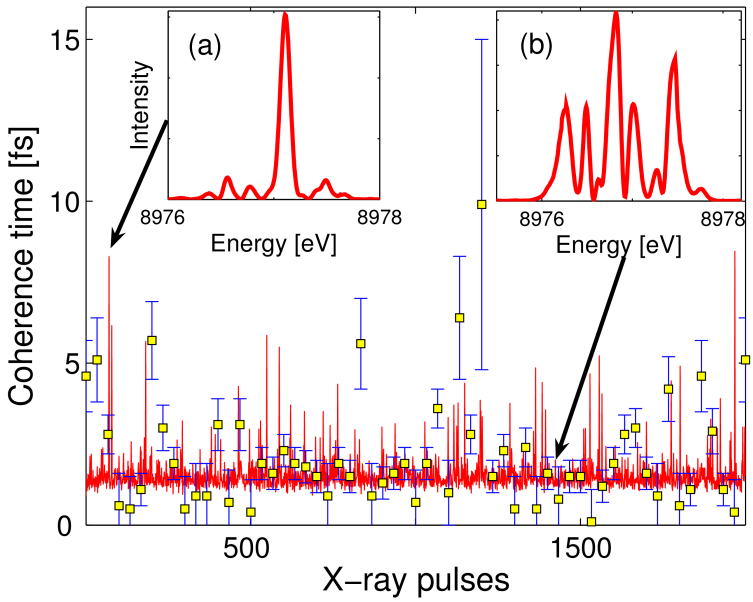

Fig. 9. Experimental measurements of the coherence time fluctuation after Si (111) monochromator (yellow) are compared to simulations (red). Inset (a) shows a simulated spectrum with a single dominant mode providing the longest coherence time. Inset (b) shows a spectrum with multiple modes overfilling the bandwidth of the monochromator that results in a relatively shorter coherence time.

spectrum according to Wiener-Khinchin theorem. Due to the complex structure in the spectrum, an evaluation of the speckle contrast requires a numerical integration. In order to quantify the effect of the spectral fluctuation on the speckle contrast, we perform the simulation by using the FEL operational parameters used in our experiment, of which details are described elsewhere [30].

Figure 10(a) shows that the contrast values from the simulation and experiment both converge to 0.26 while the experimental data displaying slightly more pronounced contrast fluctuation. The result may imply that there were possibly less number of temporal modes transmitted by the Si (111) monochromator in the experiment as compared to the simulation result. Figure 10(b) shows the probability distribution of the speckle contrast from series of FEL pulses. In both the simulation and experiment, we find that the majority of the contrast values (i.e. over 80 % and 50 % of the shots in the simulation and experiment respectively) fall in-between 0.2 and 0.3. There are rare high contrast shots whose speckle contrast β exceeds 0.4. However, it is very interesting to note that only in the experimental values, the contrasts fall below the lower limit of 0.2, which is set by the monochromator bandwidth. A possible explanation for this statistical observation is given in the later section “Effect of pulse duration on speckle contrast.”

4.4. Pulse duration measurement via temporal speckle statistics

Due to electron beam shot noise [7], the SASE light consists of random temporal spikes, of which characteristic width corresponds to the coherence time. The statistical fluctuation of the SASE radiation after a narrow-band monochromator follows the relation,

$$\sigma_W / \langle W \rangle = 1/\sqrt{M}, \tag{11}$$

#193069 - $15.00 USD Received 28 Jun 2013; revised 22 Aug 2013; accepted 15 Sep 2013; published 8 Oct 2013

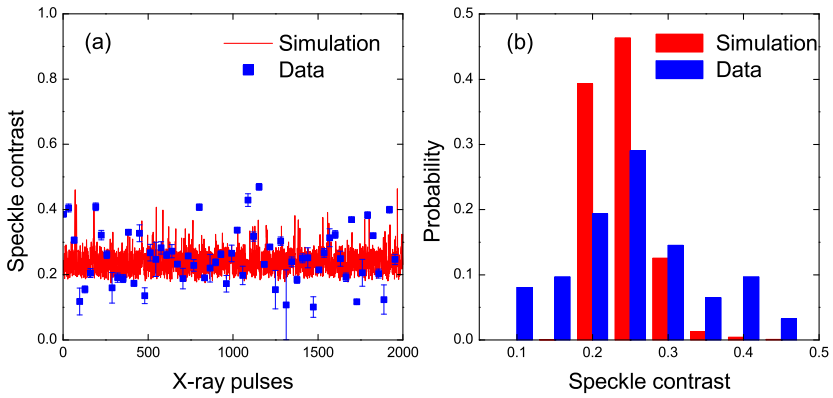

Fig. 10. (a) Comparison between the experimental result and simulation. (b) Comparison between the probability distributions of the speckle contrasts for the data and simulation.

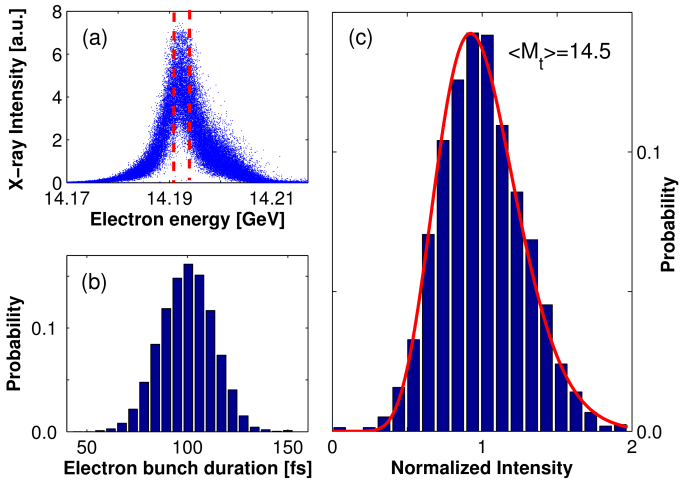

Fig. 11. (a) Intensity (blue) after Si (111) monochromator is plotted against the linac operation energy. Data points that fall between two red dash lines are used for the analysis. (b) Distribution of electron bunch width (FWHM) measured during the experiment. (c) The intensity distribution of the FEL pulses plotted with the gamma distribution fit, which yields a mode number of $\langle M_t \rangle$ = 14.5.

where W is pulse intensity, σ_W is the standard deviation of the intensity and M is a number of independent modes in the beam consisting of transverse and a longitudinal modes (i.e. $M = M_s^2 M_t$). Since the LCLS beam is transversely coherent, the RMS fluctuation primarily depends on the longitudinal modes, i.e. $M_t = T/\tau_c$ where T is the x-ray pulse duration.

The pulse-to-pulse intensity fluctuation of SASE sources such as LCLS can be described by Eq. (11), given sufficient incident photon flux. In our experiment, series of x-ray pulse intensities were monitored with a photodiode after the Si(111) monochromator. However, since the center frequency of the pink beam spectrum fluctuates due to the electron energy jitter, it is very important to bin the data in accordance with the electron energy and electron bunch width. Figure 11(a) shows the overlay between sorted electron energy and the throughput intensity of

#193069 - $15.00 USD Received 28 Jun 2013; revised 22 Aug 2013; accepted 15 Sep 2013; published 8 Oct 2013

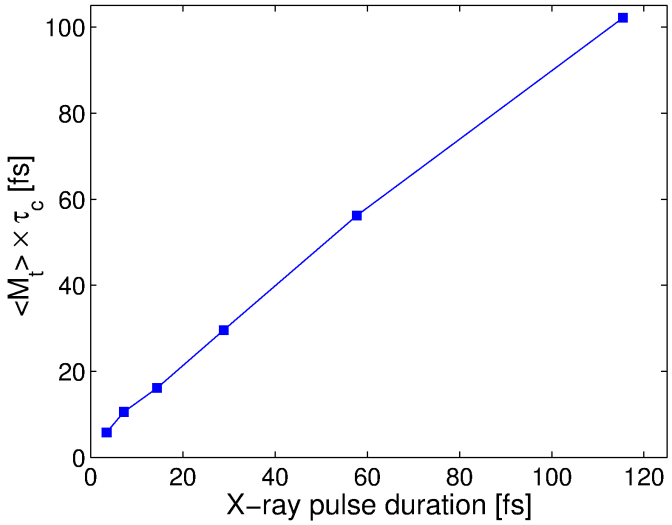

Fig. 12. (a) Simulation result shows that the x-ray pulse duration after the silicon (111) monochromator is linearly related to the product of coherence times and numbers of temporal modes . (b) Comparison between the x-ray pulse duration before and after the monochromator.

the x-ray radiation after the monocromator. For the evaluation of M_t (number of independent temporal modes), we choose the shots with the greatest energy overlap between the LCLS spectrum and the monochromator acceptance, which lie between the dashed lines. Subsequently we grouped the data set such that the electron bunch duration (measured at upstream of the experimental hall) corresponding to the sampled intensities falls within a single standard deviation of the electron bunch length distribution as shown in Fig. 11(b). Finally Fig. 11(c) shows the normalized intensity distribution of the incoming x-rays and the fit to the gamma density distribution, which yields $\langle M_t \rangle$ = 14.5. This result implies that the pulse duration of the x-rays was 29 $\pm$ 14 fs during our experiment, which is considerably shorter than the electron bunch duration of 90 fs. This observation is consistent with our simulation and results from previously reported experiments [35, 36].

A series of the 1D FEL simulations are performed to model the outcome of the coherence measurement and the number of modes from the integrated intensity for different x-ray pulse duration. Figure 12(a) shows the correlation between the x-ray pulse duration and the product of the number of the modes and coherence time. We observe that the linearity holds very well for x-ray pulses which duration is less than 100 fs. We conclude that the x-ray pulse duration can be reliably deduced by taking the product of temporal modes and the coherence time.

For a more accurate evaluation of the pulse duration, we need to account for the broadening of the pulse duration as it propagates through the silicon monochromator. The broadening of the femtosecond x-ray pulses is expected due to the path length differences between the incident and diffracted beam out of the crystal monochromator. In order to estimate the broadening effect, we follow the formulation suggested by Tomov et al. [37], in which the temporal broadening of a short laser pulse in a crystal is described by the Maxwell's equation. For a Gaussian input pulse with a FWHM width of 30 fs, we expect a temporal broadening of 5 fs from Si (111) crystal reflections as shown in Fig. 12 (b). An additional source of broadening also comes from the transient response of the crystal, which is expected to be about 5 fs [38]. A convolution of

#193069 - $15.00 USD Received 28 Jun 2013; revised 22 Aug 2013; accepted 15 Sep 2013; published 8 Oct 2013

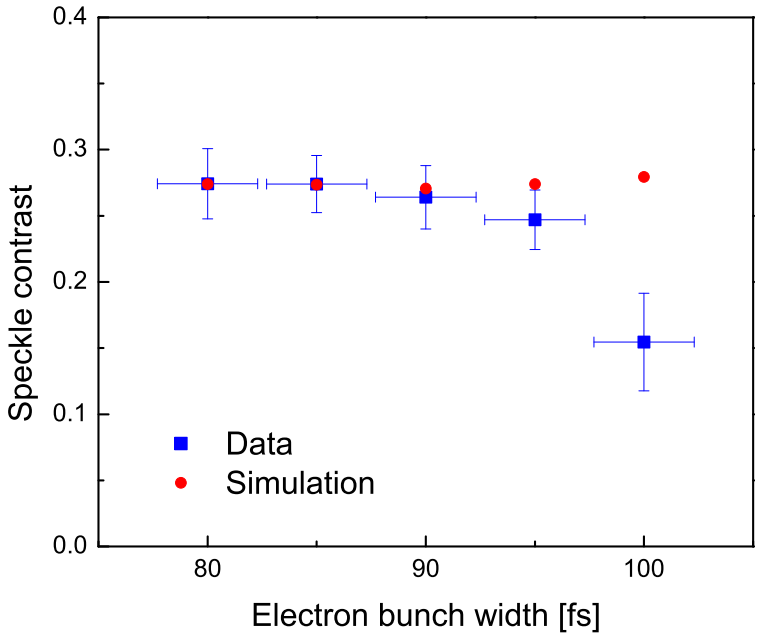

Fig. 13. Speckle contrast is plotted against electron bunch width. The speckle contrast converges to β = 0.26 for all electron bunch duration while the contrast begins to drop for the electron bunches longer then 90 fs in the experiment.

these effects leads to the final pulse duration of 31 fs that lies within uncertainty of our experimental result. This calculation merely demonstrates that the effect of pulse broadening should be negligible within the scope of our work. However, an elaborate study on temporal dependence of XFEL pulse in crystals has been reported by Lindberg et al. [39], in which the theory of dynamical x-ray diffraction was used to calculate the response of Bragg diffracted pulse on a crystal. If LCLS is operated at a considerably lower bunch charge (e.g. 20 pC instead of 200 pc) to produce sub 10 fs x-ray pulse, such pulse broadening effect needs to be accounted for.

4.5. Effect of pulse duration on speckle contrast

We correlated the speckle contrasts measured in the WAXS experiment to the LCLS electron bunch duration on a pulse-to-pulse basis. According to the simulation, the electron bunch duration is linearly proportional to the x-ray pulse duration. And also the effect of the pulse duration broadening is not significant in our case. The relation between the x-ray pulse duration and the speckle contrast can be found by sorting the speckle contrasts with respect to the electron bunch duration. Subsequently, additional sets of FEL simulations were performed using the respective electron bunch duration (100 iterations each) as the input parameters to compare with the experimental results. As shown in Fig. 13, when the bunch duration are shorter than 90 fs (approximately corresponding to 30 fs x-ray pulse duration), the data and simulation show quantitative agreements as β converges to 0.26. However when the bunch duration are longer than 90 fs, the speckle contrasts from the experiment begins to drop while the values from the simulation remains at 0.26.

In reality, the speckle contrast measured in the experiment reflects a convolution of the beam coherence and sample dynamics. Since the sample dynamics are not considered in the simu-

#193069 - $15.00 USD Received 28 Jun 2013; revised 22 Aug 2013; accepted 15 Sep 2013; published 8 Oct 2013

lation, we suspect that the discrepancy comes from possible structural changes taking place during the illumination of the x-ray pulse on the sample and thus decreasing the speckle contrast. The observed reduction in the speckle contrast at longer bunches shows that the intensity from a strong FEL pulse could induce ultrafast structural changes at the atomic-length scale, which occurs under sub-100 fs timescale.

5. Conclusion

We demonstrate that a single shot speckle visibility analysis offers a versatile and suitable ways of measuring coherence of the hard x-ray FEL pulses. In the SAXS configuration, our single shot result shows that the focused FEL beam is transversely coherent with marginal pulse-to-pulse variation. We also find that the transverse coherence along vertical direction is equivalent to the horizontal counterpart despite the anisotropy in the electron beam emittance. However, severe fluctuations of the speckle contrast are measured at an atomic length scale ($Q = 26\ \mathrm{nm}^{-1}$) after the Si (111) monochromator. Quantitative agreement between our data and the simulation confirms the mean coherence time of about 2 fs and the x-ray pulse duration of 29 fs that is 3 times shorter than the electron bunch duration at LCLS.

Finally the present work shows that, by evaluating the speckle contrast at different x-ray pulse durations, one should be able to monitor extremely fast atomic scale response. Making a time-resolved studies by varying the detector exposure time has been demonstrated previously [40]. Similarly by using femtosecond pulse durations and the peak intensity of the XFEL beam, it is possible to systematically explore ultrafast dynamics occurring at atomic length scales in amorphous systems. However since a dramatic reduction of the scattered photons is expected at high wavevectors, it is highly desirable to develop a 2D detector with much smaller pixel size and larger number of pixels to enhance the photon statistics in the analysis. Also, the availability of a seeded hard x-ray FEL [41] would be very useful for acquiring high contrast speckle images with higher photon flux.

Acknowledgments

The Linac Coherent Light Source is funded by the U.S. Department of Energy's Office of Basic Energy Sciences and led by the SLAC National Accelerator Laboratory, which is operated by Stanford University for the DoE. P. H. F. and G. B. S. were supported by the U.S. Department of Energy, Office of Basic Energy Sciences, Division of Materials Sciences and Engineering. This research was supported by the Converging Research Center Program through the Ministry of Science, ICT and Future Planning, Korea (2013K000307). The Au nanopowder samples were supplied by A. Plech. P.W., M.C.-C. We thank Y. Ding and Z. Huang for helpful discussions. The authors acknowledge financial support by the Deutsche Forschungsgemeinschaft within the framework of the graduate school 1355 Physics with new advanced coherent radiation sources.

#193069 - $15.00 USD Received 28 Jun 2013; revised 22 Aug 2013; accepted 15 Sep 2013; published 8 Oct 2013